JOURNAL OF COLLOID AND INTERFACE SCIENCE 161, 43–52 (1993)

On Mass Transfer from a Newtonian Fluid to a Swarm of Adsorbing Spheroidal Particles for High Peclet Numbers

F. A. COUTELIERIS, V. N. BURGANOS, AND A. C. PAYATAKES[1]

Department of Chemical Engineering, University of Patras, and Institute of Chemical Engineering and High Temperature Chemical Processes, GR 26500 Patras, Greece

Received March 9, 1993; accepted June 7, 1993

The problem of mass transfer from a Newtonian fluid stream to a swarm of adsorbing stationary solid spheroidal particles under creeping flow conditions is considered. The "spheroid-in-cell" model is used for the representation of the swarm and the axis of symmetry is assumed parallel to the approaching uniform stream. An analytical solution to the convective diffusion equation for high Peclet number is obtained using Levich's method. Simple analytical expressions are derived for the dimensionless concentration, the local Sherwood number, and the thickness of the diffusion layer in terms of the Peclet number, the porosity of the swarm, and the position on a meridian plane. It is found that for prolate spheroids-in-cell the diffusion film thickness is minimal at the stagnation point as in the case of spheres-in-cell. However, in the case of oblate spheroids-in-cell the diffusion layer thickness becomes minimal at positions between the stagnation point and the equator. Calculated values of the overall mass transfer coefficient indicate that the adsorption rate is higher for oblate spheroids-in-cell than for spheres-in-cell and prolate spheroids-in-cell, assuming either the same volume, or the same surface area. The mass transfer coefficient increases with decreasing porosity of the swarm for all geometries studied.

1. INTRODUCTION

Mass transfer from a moving fluid to a swarm of adsorbing stationary particles is encountered in a large number of industrial processes (chemical reactors, filters, flooding processes, etc.). Very often the particles are sufficiently small and the flow sufficiently slow to justify the assumption of creeping flow. Another assumption that can be usually made (especially in the case of liquid solutions and colloidal suspensions) is that the Peclet number is much larger than unity. Finally, the assumption that the fluid viscosity, $\tilde{\mu}$, and density, $\tilde{\rho}$, are independent of the concentration of the diffusing species makes it possible to uncouple the flow problem from the mass-transfer problem.

[1] Ed. Pls. Supply

Exact analytical solutions of the problem of creeping flow through a swarm of particles are available for the case of uniform spherical particles in a regular packing. In more complicated cases it is rather difficult to find an analytical solution. In such cases, it is often useful to use a suitable model to approximate the real flow field. A fundamental modeling concept is the representation of any particle of the swarm as a solid sphere, and the flow around it as the flow in a spherical fluid layer (of appropriate thickness) enveloping the solid sphere. The thickness of the fluid layer is adjusted so that the solid volume fraction of the cell equals the solid volume fraction of the swarm.

Happel (1) developed the prototype of a class of models that have become known as "sphere-in-cell" models. Kuwabara (2) proposed a closely related model independently. The major differences between these two models are the following two: Happel's model assumes that the outer fluid surface is stationary and that the solid sphere moves with a constant velocity. Furthermore, it assumes that the shear stress on the outer fluid surface vanishes everywhere. Kuwabara's model assumes that the solid sphere is stationary and that there is a radial velocity distribution on the outer fluid envelope corresponding to a uniform approach velocity. Furthermore, it assumes that the vorticity on the outer fluid surface (rather than the shear stress) vanishes everywhere. By superimposing a negative approach velocity on Kuwabara's solution one can obtain a flow corresponding to (but not coinciding with) that of Happel. As Tien (3) has pointed out, the two models give very similar flow fields for a wide range of porosity values.

In addition to the "sphere-in-cell" models, a similar class of models has been proposed by Happel (1) and Kuwabara (2), namely, the "cylinder-in-cell" models, which are suitable for modeling flow through fibrous mats, arrays of parallel fibers, etc.

An important improvement on the Happel and Kuwabara models was proposed by Neale and Nader (4), who considered that the basic cell is embedded into an unbounded, continuous, homogeneous, and isotropic permeable medium which has the same permeability as that of the swarm of

0021-9797/93 $5.00

particles. The flow in the exterior permeable medium is described by Brinkman's equation. This model is a combination of the Happel "sphere-in-cell" concept with the Brinkman model (5). The case of a permeable inner sphere surrounded by a free surface envelope has also been treated with a similar approach (6).

In all the aforementioned works the particles were assumed to be either spherical or cylindrical. In practice (during depth filtration or fluid–solid reaction processes, for instance), particles or grains are often nonspherical; in fact, their shape is closer to spheroidal than to spherical. Epstein and Masliyah (7) have formulated a "spheroid-in-cell" model using the zero vorticity condition of Kuwabara and the free surface condition of Happel at the outer boundary, and solved the corresponding flow problems numerically. Recently, Dassios *et al.* (8) developed an analytical series-expansion solution to the creeping flow equation in spheroids-in-cell using the zero vorticity boundary condition.

All these models are useful for examining mass transfer processes from the moving fluid to the swarm and vice versa. Pfeffer and Happel (9) and Pfeffer (10) used Happel's model to solve the problem of mass transfer to a sphere in a swarm for the case of high Peclet number, and obtained an expression of the form $Sh_o = f(\gamma)Pe^{1/3}$, where Sh_o is the overall Sherwood number, Pe is the Peclet number, and $f(\gamma)$ is a simple analytic function of the solid volume fraction, γ. This solution was obtained using the method of Levich (11), who solved the problem of high Pe mass transfer from a quiescent unbounded fluid to an adsorbing solid sphere falling through it with constant velocity. Levich showed that for $Pe \gg 1$ mass transfer occurs in a very thin concentration boundary layer near the solid sphere. He calculated the overall Sherwood number for this case, and obtained the expression $Sh_o = 0.997\ Pe^{1/3}$. The Levich solution was also obtained independently by Friedlander (12) and Lochiel and Calderbank (13), whereas a second order correction to this expression was introduced by Acrivos and Goddard (14).

Tardos *et al.* (15) obtained expressions of the form $Sh_o = 0.997g(\epsilon)Pe^{1/3}$, using the Happel, Kuwabara, and Neale and Nader models, where $g(\epsilon)$ is a model dependent function of the porosity, ϵ. These authors have pointed out that the model of Neale and Nader gives somewhat better agreement with experimental data than the other two models.

In the present work, we use the "spheroid-in-cell" model of Dassios *et al.* (8) to solve the corresponding problem of mass transfer from a spheroidal fluid envelope to an adsorbing solid spheroid (for $Re < 1$ and $Pe \gg 1$). This solution can be used to model low-Re/high-Pe mass transfer to a swarm of adsorbing spheroidal particles, in the same way in which the works of Pfeffer and Happel (9) and Tardos *et al.* (15) are used for swarms of adsorbing spheres. We provide analytical expressions for the concentration, and for the local and overall Sherwood numbers. The mass transfer occurs in a very thin boundary layer near the solid spheroid, the thickness of which is given as a function of position, Peclet number, porosity, and axis ratio for prolate and oblate spheroidal geometries.

2. FORMULATION AND SOLUTION OF THE PROBLEM: THE PROLATE-SPHEROID-IN-CELL CASE

We consider a solid spheroid with long semiaxis $\tilde{a}_3$ and short semiaxis $\tilde{a}_1$ (Fig. 1a). We consider first the case of a prolate spheroid ($\tilde{a}_3 > \tilde{a}_1$). As we see later, our results can easily be converted to the case of an oblate spheroid using a simple transformation. The semifocal length $\tilde{c}$ is defined by $\tilde{c} = (\tilde{a}_3^2 - \tilde{a}_1^2)^{1/2}$, and the eccentricity by $e = \tilde{c}/\tilde{a}_3$. We also consider a larger confocal prolate spheroidal surface with long semiaxis $\tilde{b}_3$ and short semiaxis $\tilde{b}_1$, surrounding the solid spheroid. The space between the two spheroidal surfaces is occupied by a Newtonian fluid having dynamic viscosity $\tilde{\mu}$ and density $\tilde{\rho}$. The spheroid-in-cell is used as a model for a swarm of spheroids, as in Dassios *et al.* (8). The dimensions of the outer spheroidal surface are determined so that the solid volume fraction of the spheroid-in-cell is equal to the solid volume fraction of the swarm, γ. The inner spheroid is stationary while the fluid in the cell flows past it in an upward direction. This flow is caused by a uniform stream moving at a velocity of magnitude $\tilde{u}$ (at the outer boundary) in the positive z-direction. The approaching fluid is a dilute solution of A in B, with free stream concentration $\tilde{c}_{A,\infty}$. We assume that A diffuses toward the solid surface, where it is adsorbed instantly.

For convenience, we work with dimensionless variables, using $\tilde{a}_1$ as the characteristic length, $\tilde{u}$ as the characteristic velocity, and $\tilde{c}_{A,\infty}$ as the characteristic concentration. Dimensionless variables are denoted with the same symbols as the corresponding dimensional ones but without the tilde. Assuming, now, that the physical properties of the fluid ($\tilde{\mu}$ and $\tilde{\rho}$) are independent of the concentration of A, c_A, the flow problem becomes uncoupled from the mass-transfer problem, and can be solved separately. This solution was reported in Dassios *et al.* (8) and is used here. The leading term of the solution for the stream function is given by

$$\psi(\tau, \zeta) = \frac{c^2}{D}\left[\Lambda_2 G_2(\tau) + \Lambda_3\left(\frac{5G_4(\tau_\beta)}{G_1(\tau_\beta)}G_1(\tau) + G_4(\tau)\right) + \Lambda_4 H_2(\tau)\right]G_2(\zeta), \quad [1]$$

and is known to approximate the full solution with sufficient accuracy for small and medium aspect ratios (7). Here τ and ζ are independent variables, defined by

$$\tau = \cosh \eta, \quad \zeta = \cos \theta, \quad [2]$$

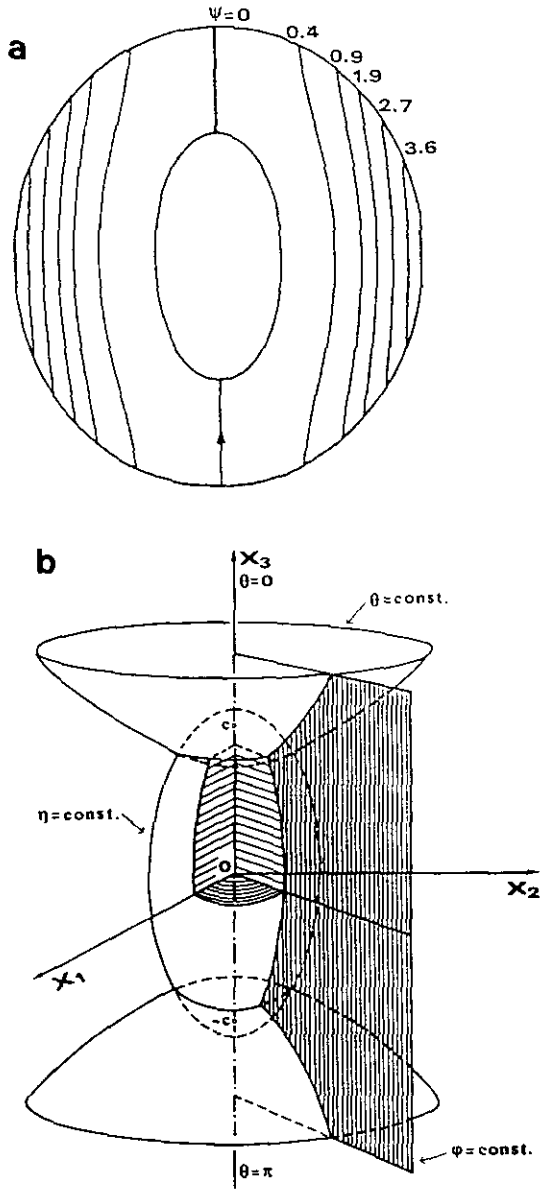

FIG. 1. Solid prolate spheroid in a confocal prolate spheroidal envelope (some characteristic stream lines are included) (a) and prolate spheroidal coordinates system (b).

where η and θ are the prolate spheroidal coordinates (Fig. 1b). $G_n(x)$ and $H_n(x)$ denote the Gegenbauer functions of the first and second kind, respectively, of degree $(-\frac{1}{2})$ and order n, where D, Λ_2, Λ_3 and Λ_4 are constants that depend on the geometry of the spheroid-in-cell (7). (For the sake of completeness, the expressions for D, Λ_2, Λ_3, and Λ_4 are given in Appendix A.) The value of τ on the solid spheroidal surface is

$$\tau_\alpha = \cosh \alpha = \frac{a_3}{c} = e^{-1} \qquad [3]$$

whereas on the outer spheroidal surface it is

$$\tau_\beta = \cosh \beta = \frac{b_3}{c}, \qquad [4a]$$

where

$$\beta = \sinh^{-1}\left(\frac{b_1}{c}\right) = \sinh^{-1}\sqrt{\left(\frac{b_3}{c}\right)^2 - 1} \qquad [4b]$$

with

$$b_3 = \left[\frac{a_3}{2\gamma} + \sqrt{\left(\frac{a_3}{2\gamma}\right)^2 - \left(\frac{c^2}{3}\right)^3}\right]^{1/3} + \left[\frac{a_3}{2\gamma} - \sqrt{\left(\frac{a_3}{2\gamma}\right)^2 - \left(\frac{c^2}{3}\right)^3}\right]^{1/3}. \qquad [5a]$$

If the expression under the square root sign is negative, then the following expression for b_3 must be used:

$$b_3 = \frac{2\sqrt{3}c}{3}\cos\left[\frac{1}{3}\cos^{-1}\left(\frac{3\sqrt{3}a_3}{2\gamma c^3}\right)\right] \qquad [5b]$$

The components of the dimensionless velocity $\mathbf{v}$ are obtained by differentiation of ψ,

$$v_\eta = \frac{1}{c^2\sqrt{\tau^2 - \zeta^2}\sqrt{\tau^2 - 1}}\frac{\partial \psi}{\partial \zeta} \qquad [6a]$$

$$v_\theta = \frac{1}{c^2\sqrt{\tau^2 - \zeta^2}\sqrt{1 - \zeta^2}}\frac{\partial \psi}{\partial \tau}. \qquad [6b]$$

Assuming pseudo-steady state in the mass transport problem (as was also done in solving the flow problem), and that the diffusion coefficient and total concentration are constant, the equation governing the convective diffusion of A becomes

$$\mathbf{v} \cdot \nabla c_A = \mathrm{Pe}^{-1}\nabla^2 c_A \qquad [7]$$

with $\mathrm{Pe} = \tilde{u}\tilde{a}_1/\tilde{\mathcal{D}}_{AB}$.

For $\mathrm{Pe} \gg 1$ the thickness of the concentration boundary layer is negligible compared to the local radius of curvature of the particle. Neglecting the curvature term, invoking the axial symmetry, and using prolate spheroidal coordinates, Eq. [7] becomes

$$v_\eta\sqrt{\tau^2 - 1}\frac{\partial c_A}{\partial \tau} - v_\theta\sqrt{1 - \zeta^2}\frac{\partial c_A}{\partial \zeta} = \frac{\mathrm{Pe}^{-1}\sqrt{\tau^2 - 1}}{c\sqrt{\tau^2 - \zeta^2}}\frac{\partial}{\partial \tau}\left[\sqrt{\tau^2 - 1}\frac{\partial c_A}{\partial \tau}\right]. \qquad [8]$$

This equation is to be integrated with the following boundary conditions:

$$\text{B.C.1: } c_A = 0 \qquad \text{on } \tau = \tau_\alpha \qquad [9]$$

$$\text{B.C.2: } c_A = 1 \qquad \text{as } \tau \to \infty \qquad [10]$$

$$\text{B.C.3: } c_A \text{ is finite} \qquad \text{as } \zeta \to -1 \ (\tau \neq \tau_\alpha). \qquad [11]$$

By replacing τ- with ψ-differentiation (von Mises transformation), Eq. [8] becomes

$$\frac{\partial c_A}{\partial \zeta} = -\mathrm{Pe}^{-1} c^3 (\tau^2 - 1) \frac{\partial}{\partial \psi}\left[v_\theta \sqrt{1-\zeta^2}\sqrt{\tau^2-\zeta^2}\, \frac{\partial c_A}{\partial \psi}\right]_\zeta \qquad [12]$$

The concentration boundary layer is expected to be thin for $\mathrm{Pe} \gg 1$, which justifies the use of B.C.2 in the convenient form of Eq. [10], rather than as $c_A = 1$ on $\tau = \tau_\beta$. Defining a new variable $y = \tau - \tau_\alpha$, we have $y \ll \tau_\alpha$ in the region of interest. It is simple to show, using second order expansion in y, that in this region Eq. [1] can be written as

$$\psi \approx -\frac{c^2}{D} E y^2 G_2(\zeta); \quad y \ll \tau_\alpha \qquad [13]$$

with

$$E = \frac{\Lambda_2}{2} + \frac{15}{4}\Lambda_3 \tau_\alpha^2 - \frac{3\Lambda_3}{4} + \frac{\Lambda_4}{4}\ln\frac{\tau_\alpha + 1}{\tau_\alpha - 1} - \frac{\Lambda_4}{2}\frac{\tau_\alpha}{\tau_\alpha^2 - 1}. \qquad [14]$$

Substituting ψ from Eq. [13] into Eq. [6b] and then replacing y by its expression in terms of ψ, one obtains

$$v_\theta = \frac{1}{\sqrt{\tau^2 - \zeta^2}} \sqrt{\frac{2E}{c^2 D}}\sqrt{-\psi}. \qquad [15]$$

Equations [12] and [15] give

$$\frac{\partial c_A}{\partial \zeta} = -\mathrm{Pe}^{-1} c^2 (\tau_\alpha^2 - 1)\sqrt{\frac{2E}{D}} \times \sqrt{1-\zeta^2}\, \frac{\partial}{\partial \psi}\left[\sqrt{-\psi}\, \frac{\partial c_A}{\partial \psi}\right]. \qquad [16]$$

The boundary conditions become

$$\text{B.C.1: } c_A = 0 \qquad \text{on } \psi = 0 \qquad [17]$$

$$\text{B.C.2: } c_A = 1 \qquad \text{as } \psi \to -\infty \qquad [18]$$

$$\text{B.C.3: } c_A \text{ is finite} \qquad \text{as } \zeta \to -1 \ (\psi \neq 0). \qquad [19]$$

If we define a new variable, t, by

$$t = -\mathrm{Pe}^{-1} c^2 (\tau_\alpha^2 - 1)\sqrt{\frac{2E}{D}} \int_{-1}^{\zeta} \sqrt{1-\zeta'^2}\, d\zeta', \qquad [20]$$

Equation [16] is transformed to

$$\frac{\partial c_A}{\partial t} = \frac{\partial}{\partial \psi}\left[\sqrt{-\psi}\, \frac{\partial c_A}{\partial \psi}\right], \qquad [21]$$

which is identical to that obtained by Levich (11) in solving the problem for a single sphere. Since the B.C.'s, [17]–[19], are also the same as those in the Levich problem, the concentration in the fluid phase can be directly expressed as

$$c_A(z) = \frac{1}{1.17}\int_0^z \exp\left(-\frac{4}{9} z'^3\right) dz', \qquad [22]$$

where z is an appropriately defined variable. In the prolate-spheroid-in-cell case, z is defined as

$$z = \sqrt[3]{\frac{cE\,\mathrm{Pe}}{4D(\tau_\alpha^2 - 1)}}\, y f(\zeta) \qquad [23]$$

with

$$f(\zeta) = \frac{\sqrt{1-\zeta^2}}{\{\zeta\sqrt{1-\zeta^2}/2 - (1/2)\cos^{-1}\zeta\}^{1/3}}. \qquad [24]$$

It can easily be shown that as the inner and outer spheroidal surfaces become spherical, the present solution reduces to the corresponding expression of Tardos *et al.* (15) for the Kuwabara model.

Determination of the Local and Overall Sherwood Numbers for Prolate Spheroids

For small concentrations of A in the fluid phase, the molar flux of A is given by

$$\tilde{\mathbf{N}}_A = -\tilde{\mathcal{D}}_{AB}\nabla \tilde{c}_A, \qquad [25]$$

where $\tilde{\mathcal{D}}_{AB}$ is the molecular diffusivity of A in B. The normal component of the diffusive flux at the solid surface is

$$-\tilde{N}_{Ay})_{y=0} = \left(\frac{\tilde{\mathcal{D}}_{AB}\tilde{c}_{A,\infty}}{\tilde{a}_1}\frac{\sqrt{\tau_\alpha^2 - 1}}{c\sqrt{\tau_\alpha^2 - \zeta^2}}\frac{\partial c_A}{\partial y}\right)_{y=0}. \qquad [26]$$

It can also be expressed as

$$-\tilde{N}_{Ay})_{y=0} = \tilde{k}(\tilde{c}_{A,\infty} - \tilde{c}_{A,s}), \quad [27]$$

where $\tilde{k}$ is the local mass transfer coefficient. Using $\tilde{c}_{A,s} = 0$, the expression for the local Sherwood number is

$$\mathrm{Sh}(\zeta) \equiv \frac{\tilde{k}\tilde{a}_1}{\tilde{\mathcal{D}}_{AB}} = 0.538\sqrt[3]{\frac{E(\tau_\alpha^2 - 1)^{1/2}}{c^2 D}}\frac{f(\zeta)}{\sqrt{\tau_\alpha^2 - \zeta^2}}\mathrm{Pe}^{1/3}. \quad [28]$$

The overall Sherwood number is defined as

$$\mathrm{Sh}_o \equiv \frac{\tilde{k}_o\tilde{a}_1}{\tilde{\mathcal{D}}_{AB}}, \quad [29]$$

where $\tilde{k}_o$ is the overall mass transfer coefficient determined from

$$\tilde{k}_o(\tilde{c}_{A,\infty} - \tilde{c}_{A,s})\tilde{S}_{ps} = -\int_{\tilde{S}_{ps}} \tilde{N}_{Ay})_{y=0}\, d\tilde{S}. \quad [30]$$

In Eq. [30], S_{ps} is the area of the prolate spheroidal solid surface (at $\tau = \tau_\alpha$),

$$\tilde{S}_{ps} = 2\pi\tilde{a}_1^2\left(1 + \frac{a_3}{e}\sin^{-1}e\right),$$

and $d\tilde{S}$ is a spheroidal surface element given by

$$d\tilde{S} = -\tilde{a}_1^2 c^2\sqrt{(\tau^2 - \zeta^2)(\tau^2 - 1)}\, d\zeta d\phi$$

with ϕ the azimuthal angle. Straightforward manipulation of Eq. [30] leads to

$$\mathrm{Sh}_o = \frac{3.383}{S_{ps}}\sqrt[3]{\frac{c^4 E(\tau_\alpha^2 - 1)^2}{D}}\int_1^{-1} f(\zeta)d\zeta\,\mathrm{Pe}^{1/3}, \quad [31a]$$

where $S_{ps} = \tilde{S}_{ps}/\tilde{a}_1^2$.

By defining the function

$$g_{ps}(\gamma, a_3) = \frac{3.383}{S_{ps}}\sqrt[3]{\frac{c^4 E(\tau_\alpha^2 - 1)^2}{D}}\int_1^{-1} f(\zeta)d\zeta, \quad [32]$$

Eq. [31a] can be written as

$$\mathrm{Sh}_o = 0.997 g_{ps}(\gamma, a_3)\mathrm{Pe}^{1/3}, \quad [31b]$$

which can be considered as a generalization of the equation derived by Tardos *et al.* (15) for spheres. It is important to note that Sh_o depends not only on γ and Pe, but also on the dimensionless axis ratio of the spheroidal particles, a_3. Note that γ can be replaced by the porosity ($\epsilon = 1 - \gamma$). Calculated values of the function $g_{ps}(\gamma, a_3)$ for several axis ratio and solid fraction values are given in Table 1.

For practical calculations, the diffusion film thickness can be estimated from the Nernst approximation

$$\tilde{\delta}(\zeta) = \frac{\tilde{\mathcal{D}}_{AB}}{\tilde{k}(\zeta)} \quad [33]$$

and, using dimensionless quantities,

$$\delta(\zeta) = \mathrm{Sh}(\zeta)^{-1}. \quad [34]$$

The dimensionless local mass transfer coefficient, then, is given simply by

$$k(\zeta) = \frac{\tilde{k}(\zeta)}{\tilde{u}} = \frac{1}{\delta(\zeta)\mathrm{Pe}}. \quad [35]$$

3. THE OBLATE-SPHEROID-IN-CELL CASE

The oblate-shaped-in-cell case ($\tilde{a}_1 > \tilde{a}_3$) can be treated by means of the transformation (16)

$$\tau = i\bar{\tau} \Rightarrow \bar{\tau} = -i\tau \quad [36a]$$

$$c = -i\bar{c} \Rightarrow \bar{c} = ic, \quad [36b]$$

where $\bar{c}$ is the dimensionless semifocal length in the oblate case and $\bar{\tau}$ is constant on oblate spheroidal surfaces. The convective diffusion equation (Eq. [16] in the prolate case) becomes

$$\frac{\partial c_A}{\partial\zeta} = -\mathrm{Pe}^{-1}\bar{c}^2(\bar{\tau}_\alpha^2 + 1) \times\sqrt{\frac{2\bar{E}}{\bar{D}}}\sqrt{1 - \zeta^2}\frac{\partial}{\partial\psi'}\left[\sqrt{-\bar{\psi}'}\frac{\partial c_A}{\partial\psi'}\right], \quad [37]$$

where

$$\bar{\psi} \approx -\frac{\bar{c}^2}{\bar{D}}\bar{E}\bar{y}^2 G_2(\zeta), \quad [38]$$

and the bar denotes quantities corresponding to the oblate-spheroid-in-cell case. Direct application of the transformation [36a], [36b] to the E, D expressions produces the corresponding expressions for $\bar{E}$, $\bar{D}$ (see Appendix B).

Using the complete analogy of the diffusion equation and the accompanying boundary conditions for oblate spheroids to those for prolate spheroids, one can derive analytical

TABLE 1
Values of $g_{ps}(\gamma, a_3)$ and $g_{os}(\gamma, a_3)$ for Some Characteristic Values of γ and a_3

	a_3									
γ	2.0	1.5	1.25	1.1	1.0	0.9	0.8	0.7	0.6	0.5
0[a]	0.4912	0.5501	0.5862	0.6099	0.6269	0.6432	0.6598	0.6753	0.6885	0.6970
0.0025	0.5360	0.6000	0.6407	0.6676	0.6867	0.7059	0.7255	0.7445	0.7616	0.7747
0.0050	0.5500	0.6164	0.6579	0.6857	0.7050	0.7257	0.7463	0.7665	0.7849	0.7996
0.0075	0.5606	0.6283	0.6707	0.6993	0.7198	0.7405	0.7619	0.7830	0.8025	0.8185
0.01	0.5694	0.6382	0.6815	0.7106	0.7317	0.7529	0.775	0.7968	0.8173	0.8343
0.0125	0.5772	0.6469	0.6909	0.7207	0.7420	0.7639	0.7865	0.8091	0.8303	0.8482
0.015	0.5842	0.6549	0.6995	0.7297	0.7515	0.7738	0.7970	0.8202	0.8422	0.8610
0.0175	0.5908	0.6622	0.7074	0.7381	0.7604	0.7830	0.8067	0.8304	0.8531	0.8728
0.02	0.5969	0.6691	0.7149	0.7460	0.7685	0.7916	0.8157	0.8401	0.8634	0.8838
0.03	0.6186	0.6934	0.7412	0.7738	0.7976	0.8221	0.8479	0.8742	0.8999	0.9232
0.04	0.6375	0.7145	0.7639	0.7980	0.8230	0.8486	0.8759	0.9039	0.9317	0.9578
0.05	0.6548	0.7337	0.7848	0.8200	0.8459	0.8727	0.9014	0.9310	0.9608	0.9814
0.06	0.6709	0.7517	0.8042	0.8406	0.8673	0.8953	0.9252	0.9564	0.9881	1.0186
0.07	0.6862	0.7688	0.8226	0.8600	0.8878	0.9167	0.9478	0.9805	1.0139	1.0468
0.08	0.7010	0.7853	0.8404	0.8788	0.9074	0.9373	0.9696	1.0037	1.0389	1.0739
0.09	0.7154	0.8012	0.8576	0.8971	0.9255	0.9573	0.9908	1.0263	1.0633	1.1004
0.1	0.7294	0.8168	0.8744	0.9149	0.9451	0.9768	1.0114	1.0483	1.0870	1.1264
0.11	0.7432	0.8321	0.8909	0.9323	0.9633	0.9959	1.0317	1.0699	1.1104	1.1519
0.12	0.7568	0.8472	0.9072	0.9495	0.9813	1.0149	1.0517	1.0914	1.1335	1.1771
0.13	0.7702	0.8621	0.9233	0.9666	0.9991	1.0336	1.0715	1.1125	1.1563	1.2021
0.14	0.7836	0.8769	0.9392	0.9835	1.0166	1.0521	1.0912	1.1335	1.1790	1.2270
0.15	0.7969	0.8917	0.9551	1.0003	1.0343	1.0706	1.1108	1.1545	1.2017	1.2518
0.16	0.8102	0.9064	0.9710	1.0170	1.0519	1.0891	1.1303	1.1754	1.2243	1.2767
0.17	0.8235	0.9212	0.9869	1.0338	1.0694	1.1075	1.1498	1.1963	1.2469	1.3015
0.18	0.8368	0.9359	1.0027	1.0506	1.0868	1.1259	1.1694	1.2172	1.2696	1.3264
0.19	0.8502	0.9507	1.0187	1.0657	1.1045	1.1444	1.1890	1.2382	1.2924	1.3515
0.20	0.8636	0.9656	1.0347	1.0844	1.1224	1.1630	1.2087	1.2593	1.3153	1.3767

[a] Our asymptotic results for any axis ratio as $\gamma \to 0$ are in excellent agreement with those predicted by using the Happel and Brenner streamfunction solution (16) for a solid spheroid immersed in an unbounded fluid that approaches in the direction of the axis of symmetry.

expressions for the local concentration of component A, for the local and overall Sherwood number, and for the film thickness. For the sake of brevity, we quote here only the final forms of these expressions:

$$c_A(\bar{z}) = \frac{1}{1.15}\int_0^{\bar{z}} \exp\left(-\frac{4}{9}z'^3\right)dz', \qquad [39]$$

with

$$\bar{z} = \sqrt[3]{\frac{\bar{c}\bar{E}\,\mathrm{Pe}}{4\bar{D}(\bar{\tau}_\alpha^2+1)}}\,\bar{y}f(\zeta), \qquad [40]$$

$$\mathrm{Sh}(\zeta) = 0.538\sqrt[3]{\frac{\bar{E}(\bar{\tau}_\alpha^2+1)^{1/2}}{\bar{c}^2\bar{D}}}\,\frac{f(\zeta)}{\sqrt{\bar{\tau}_\alpha^2+\zeta^2}}\,\mathrm{Pe}^{1/3}, \qquad [41]$$

$$\mathrm{Sh}_o = \frac{3.383}{S_{os}}\sqrt[3]{\frac{\bar{c}^4\bar{E}(\bar{\tau}_\alpha^2+1)^2}{\bar{D}}}\int_1^{-1} f(\zeta)d\zeta\,\mathrm{Pe}^{1/3}, \qquad [42a]$$

with

$$S_{os} = 2\pi + \pi\frac{a_3^2}{\bar{e}}\ln\frac{1+\bar{e}}{1-\bar{e}}$$

the dimensionless area of the oblate spheroid surface and $\bar{e} = \tilde{\bar{c}}/\tilde{a}_3$ the eccentricity of the oblate spheroid. By defining the function

$$g_{os}(\gamma, a_3) = \frac{3.383}{S_{os}}\sqrt[3]{\frac{\bar{c}^4\bar{E}(\bar{\tau}_\alpha^2+1)^2}{\bar{D}}}\int_1^{-1} f(\zeta)d\zeta, \qquad [43]$$

Eq. [42a] can be written as

$$\mathrm{Sh}_o = 0.997 g_{os}(\gamma, a_3)\mathrm{Pe}^{1/3}; \qquad [42b]$$

that is, in a form similar to that of Eq. [31b]. Here, too, one can use $\epsilon\,(=1-\gamma)$ and $\bar{c}\,(=\sqrt{1-a_3^2})$ instead of γ and a_3. Table 1 presents numerical values of the function $g_{os}(\gamma, a_3)$

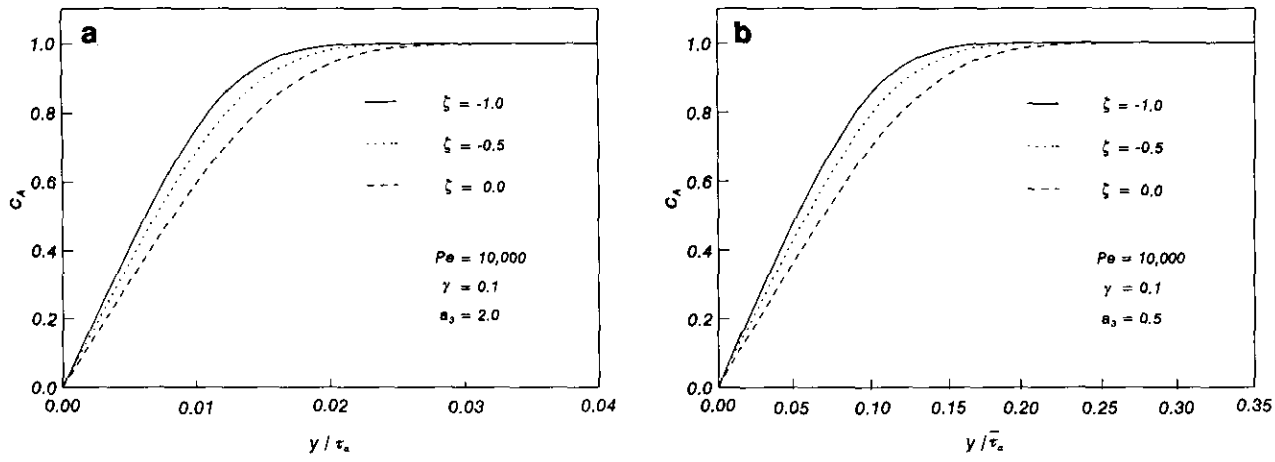

FIG. 2. Concentration profiles in the vicinity of adsorbing prolate (a) and oblate (b) spheroids-in-cell at three different angular positions on a meridian plane.

for practical values of the solid fraction and the axis ratio ($a_3 < 1$).

4. RESULTS AND DISCUSSION

Figures 2a, b show the concentration profiles for component A at different angular (ζ) positions on a meridian plane of prolate- and oblate-spheroid-in-cell systems. We note that in the prolate-spheroid-in-cell case the concentration approaches its bulk value at quite small values of y/τ_α and, hence, the assumption $y \ll \tau_\alpha$ used in the model development is satisfied with good accuracy. The analysis in the oblate-spheroid-in-cell case seems to be less accurate since the concentration approaches its bulk value at y/τ_α values of the order of 0.25. Nevertheless, our approximation to the leading term of the full stream function solution was to second order in y and the error involved for the particular Pe values is not very significant for practical applications.

The ζ-dependence of the local mass transfer coefficient in the prolate- and oblate-spheroid-in-cell cases is shown in Figs. 3a and b, respectively, for two Pe values. In the prolate case k decreases monotonically as the distance from the stagnation point ($\zeta = -1$) increases, tending to zero at the downstream stagnation point. This observation is in accord with the behavior of the diffusion layer thickness shown in the inset. Note that the diffusion layer has been magnified in the insets of Figs. 3a, b by a factor of 4 for easier reading. As the Pe value decreases, the diffusion film becomes thicker and k increases (dashed curves in Fig. 2). This seemingly strange behavior of k is caused by the fact that the approach velocity, $\tilde{u}$, has been used to render the mass transfer coefficient dimensionless, Eq. [35]; hence, a decrease in the Pe value (for

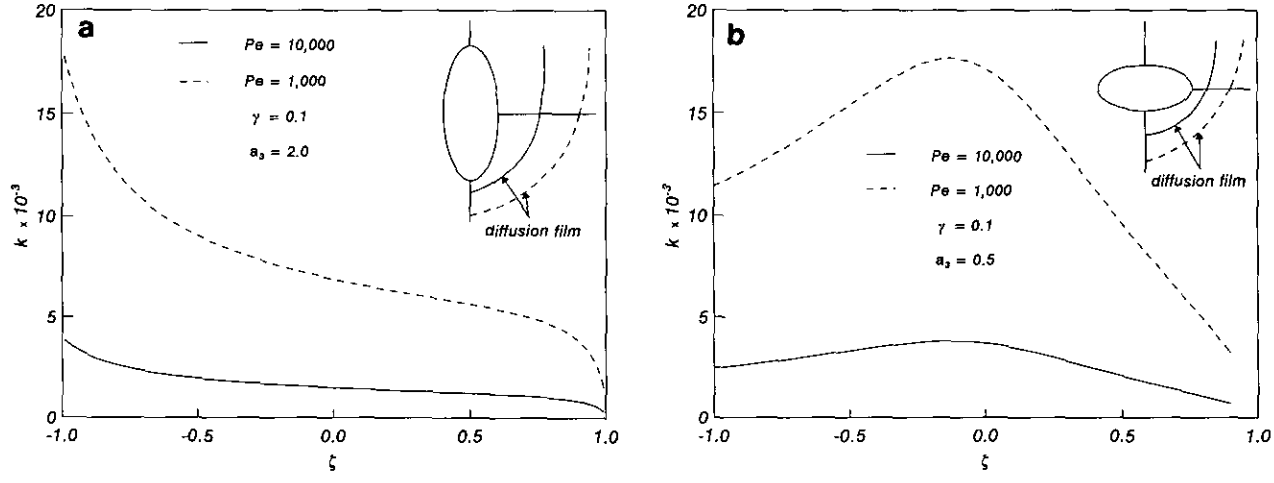

FIG. 3. Profile of the local mass transfer coefficient and of the diffusion layer (inset) along a meridian of prolate (a) and oblate (b) spheroids in cells. Variation with the Pe value. (The diffusion film has been magnified by a factor of 4 for clarity.)

fixed $\tilde{u}$) must be interpreted as an increase in the $\tilde{\mathcal{D}}_{AB}$ value which, in turn, translates to reduced diffusional resistance.

The ζ-dependence of the mass transfer coefficient in the oblate-spheroid-in-cell case is significantly different from that in the prolate-spheroid-in-cell and warrants special attention. The mass transfer coefficient k has a maximum at a position upstream of but close to the equator ($\zeta = 0$). Accordingly, the diffusion layer thickness attains its minimal value at a position near the equator and not at the upstream stagnation point, as it is the case for spherical and prolate spheroidal geometries. This new and very interesting result is *not* in conflict with the c_A vs. $\bar{y}/\bar{\tau}_\alpha$ graph of Fig. 2b, as one might think based on the increased slopes in the concentration profiles as the stagnation point is approached. It must be stressed that Fig. 2b shows the dependence of c_A on $\bar{\tau}$ values which, in order to be converted into actual distance, must be multiplied by a ζ-dependent factor. Equivalently, although the slope of the c_A curve of Fig. 2b, $dc_A/d\bar{y}$, is a measure of the diffusion flux for a given ζ value, it must be combined with a ζ-dependent quantity to compare fluxes at different ζ positions (see Eq. [26] for the corresponding flux expression in the prolate case).

Figure 4 shows the dependence of the dimensionless quantity $\mathrm{Sh_o Pe^{-1/3}}$ on the aspect ratio, $a_3 = \tilde{a}_3/\tilde{a}_1$, for spheroids-in-cell. For constant Pe, the overall Sherwood number decreases monotonically with increasing aspect ratio. This indicates that the diffusional resistance in a prolate-spheroid-in-cell is larger than that in the sphere-in-cell and in any oblate-spheroid-in-cell of the same porosity. This behavior can be explained as follows. The characteristic length used in the $\mathrm{Sh_o}$ expression is the length of the semiaxis, $\tilde{a}_1$, which is kept constant when the aspect ratio is varied (inset in Fig. 4). Therefore, the behavior of $\mathrm{Sh_o}$ is identical to that of k_o, which, in turn, is the average value of the local mass transfer coefficient, $\tilde{k}(\zeta)$, weighted by the local surface area. Direct comparison of Figs. 3a and b shows that $\tilde{k}(\zeta)$ is considerably

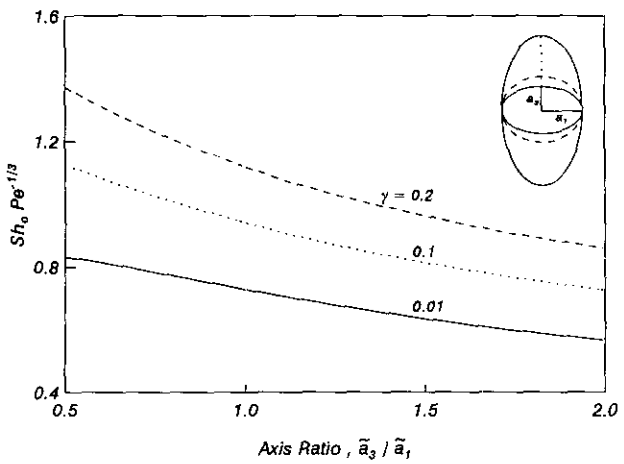

FIG. 4. Dependence of the quantity $\mathrm{Sh_o Pe^{-1/3}}$ on the axis ratio, $\tilde{a}_3/\tilde{a}_1$, for oblate and prolate spheroids-in-cell. Variation with the solid fraction, γ.

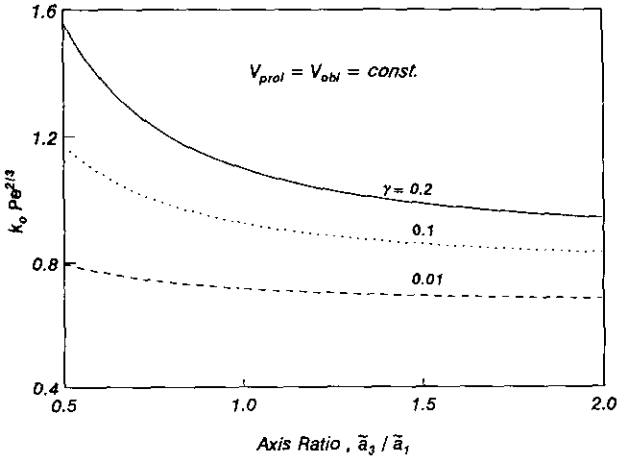

FIG. 5. Dependence of the quantity $k_o\mathrm{Pe}^{2/3}$ on the axis ratio, $\tilde{a}_3/\tilde{a}_1$, for spheroids-in-cell of the same solid volume and the same porosity. Variation with the solid fraction, γ.

higher in the oblate case than in the prolate one near the equatorial zone. The surface area per unit ζ in this region is much higher than that near the edges of the spheroid and the corresponding large $\tilde{k}$ value weighs heavily in the calculation of the overall transfer coefficient, k_o. On the other hand, as the solid fraction γ increases, the overall Sherwood number increases for constant Pe for any value of the aspect ratio. The reason for this can be traced to the development of steeper concentration profiles as the envelop decreases in size, which, in turn, is caused by increased local velocities and thinner fluid layers. This result is in qualitative accord with that implied by the expression of Tardos *et al.* (15) for spherical geometry.

Figures 5 and 6 show the effect of the aspect ratio, $a_3 = \tilde{a}_3/\tilde{a}_1$, on the quantity $k_o\mathrm{Pe}^{2/3}$ for constant volume and for constant surface area of the solid spheroid, respectively,

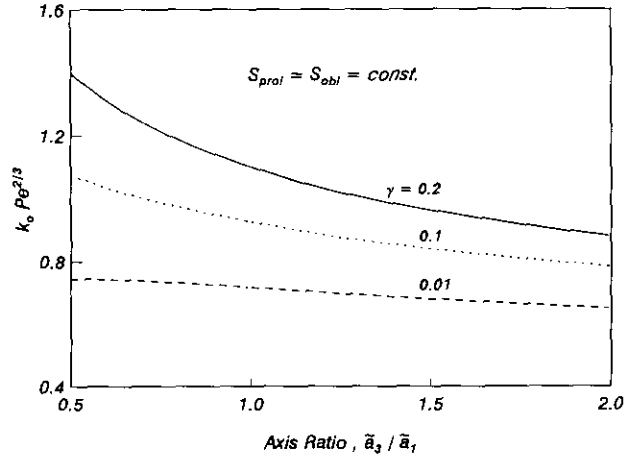

FIG. 6. Dependence of the quantity $k_o\mathrm{Pe}^{2/3}$ on the axis ratio, $\tilde{a}_3/\tilde{a}_1$, for spheroids-in-cell of the same solid surface area and the same porosity. Variation with the solid fraction, γ.

keeping the solid fraction of the cell at a fixed value. (As the different cells in these figures have different characteristic lengths, use of Sh_0 to measure diffusional limitations in this part of our work might prove misleading and has been replaced by the use of k_0 instead.) Figures 5 and 6 show that, for constant Pe, adsorption of the component A from the fluid stream on the solid surface is facilitated considerably by shaping the swarm particles as oblate spheroids rather than as spheres or prolate spheroids. In the constant volume case in particular, the mass transfer rate is almost doubled upon changing the aspect ratio from 2 to 1/2 (Fig. 5). Less drastic, though still significant, is this increase when the surface area of the solid spheroid is kept constant (Fig. 6). In general, the overall mass transfer coefficient increases as the aspect ratio a_3 decreases (as the oblate character increases), and as the solid volume fraction increases.

5. CONCLUSIONS

The problem of mass transfer from a moving fluid to a swarm of adsorbing stationary spheroidal particles is solved using a spheroid-in-cell type of model. The flow field solution under creeping conditions has been obtained by Dassios *et al.* (8) using the stream function formulation, and assuming uniform approach velocity and vanishing vorticity on the outer fluid envelope. The leading term of this series expansion solution was used here to derive a practical, yet sufficiently accurate, expression for the local velocity in spheroidal coordinates. The convective diffusion equation for a trace component (constant total concentration, constant diffusion coefficient) is then solved analytically using the von Mises transformation and assuming instantaneous adsorption at the solid surface. Simple analytical expressions are derived for the local concentration, the local and overall mass transfer coefficients, the thickness of the concentration layer around the solid spheroid, and the local and overall Sherwood numbers. The diffusion layer in prolate cells is thinnest at the forward stagnation point and grows thicker as the tail-section of the cell is approached. Oblate cells behave differently: the concentration film thickness attains a minimal value at a point upstream of but close to the equator of the solid spheroid.

According to the model predictions, oblate-spheroids-in-cell adsorb faster than spheres-in-cell or prolate-spheroids-in-cell when exposed to a fluid stream that approaches in the direction of the axis of symmetry. It was found that changing the shape of a spheroid-in-cell from prolate to oblate with the same large-to-small-axis ratio, keeping the solid volume and the porosity constant, may increase the mass transfer rate by a factor of 2 or more depending on the porosity of the cell (or, equivalently, on the solid fraction of the swarm). The corresponding increase of the mass transfer rate when the surface area is kept constant is less pronounced but remains considerable for any practical value of swarm porosity and of particle aspect ratio.

APPENDIX A

Expressions for the constants D, Λ_2, Λ_3, and Λ_4 appearing in the stream function solution (Eqs. [1], [13]):

$$D = \frac{1}{2G_2(\tau_\beta)} \times \det \begin{bmatrix} G_2(\tau_\alpha) & \left[G_4(\tau_\alpha) + \frac{5\tau_\alpha}{\tau_\beta} G_4(\tau_\beta)\right] & H_2(\tau_\alpha) \\ G_2'(\tau_\alpha) & \left[G_4'(\tau_\alpha) + \frac{5}{\tau_\beta} G_4(\tau_\beta)\right] & H_2'(\tau_\alpha) \\ G_2(\tau_\beta) & 6G_4(\tau_\beta) & H_2(\tau_\beta) \end{bmatrix} \quad [A.1]$$

$$\Lambda_2 = G_4(\tau_\alpha)H_2'(\tau_\alpha) - G_4'(\tau_\alpha)H_2(\tau_\alpha) - \frac{5}{\tau_\beta} G_4(\tau_\beta)[H_2(\tau_\alpha) - \tau_\alpha H_2'(\tau_\alpha)] \quad [A.2]$$

$$\Lambda_3 = G_2'(\tau_\alpha)H_2(\tau_\alpha) - G_2(\tau_\alpha)H_2'(\tau_\alpha) = -\frac{1}{2} \quad [A.3]$$

$$\Lambda_4 = G_2(\tau_\alpha)G_4'(\tau_\alpha) - G_2'(\tau_\alpha)G_4(\tau_\alpha) + \frac{5}{\tau_\beta} G_4(\tau_\beta)[G_2(\tau_\alpha) - \tau_\alpha G_2'(\tau_\alpha)]. \quad [A.4]$$

APPENDIX B

Expressions for the constants $\bar{\Lambda}_2$, $\bar{\Lambda}_3$, $\bar{\Lambda}_4$, $\bar{D}$, and $\bar{E}$ in the case of oblate spheroids:

$$\bar{\Lambda}_2 = \left[-\frac{1}{8}(5\bar{\tau}_\alpha^2 + 1)(\bar{\tau}_\alpha^2 + 1) + \frac{\bar{\tau}_\alpha^2(5\bar{\tau}_\alpha^2 + 3)}{4} - \frac{5}{16\bar{\tau}_\beta}(5\bar{\tau}_\beta^2 + 1)(\bar{\tau}_\beta^2 + 1)\bar{\tau}_\alpha\right][1 - \bar{\tau}_\alpha \cot^{-1}(\bar{\tau}_\alpha)] - \left[\frac{\bar{\tau}_\alpha}{4}(5\bar{\tau}_\alpha^2 + 3) + \frac{5(5\bar{\tau}_\beta^2 + 1)(\bar{\tau}_\beta^2 + 1)}{16\bar{\tau}_\beta}\right] \times \cot^{-1}(\bar{\tau}_\alpha) \quad [B.1]$$

$$\bar{\Lambda}_3 = \Lambda_3 = \frac{1}{2} \quad [B.2]$$

$$\bar{\Lambda}_4 = \frac{i}{4}(1 + \bar{\tau}_\alpha^2)\bar{\tau}_\alpha(5\bar{\tau}_\alpha^2 + 3) - \frac{i\bar{\tau}_\alpha}{8}(5\bar{\tau}_\alpha^2 + 1)(\bar{\tau}_\alpha^2 + 1) + \frac{5i}{8\bar{\tau}_\beta}(5\bar{\tau}_\beta^2 + 1)(\bar{\tau}_\beta^2 + 1)\left(\frac{1}{2} - \frac{\bar{\tau}_\alpha^2}{2}\right) \quad [B.3]$$

$$\bar{E} = \frac{\bar{\Lambda}_2}{2} - \frac{15}{4}\bar{\Lambda}_3\bar{\tau}_\alpha^2 - \frac{3\bar{\Lambda}_3}{4} - \frac{1}{2}\bar{\Lambda}_4 i\cot^{-1}(\bar{\tau}_\alpha) - \frac{\bar{\Lambda}_4}{2}\frac{\bar{\tau}_\alpha}{\bar{\tau}_\alpha^2+1} \quad [B.4]$$

$$\bar{D} = \frac{1}{(1+\bar{\tau}_\beta^2)}\left\{\frac{1}{2}(1+\bar{\tau}_\alpha^2)\left[H_2(\bar{\tau}_\beta)\left(-G_4'(\bar{\tau}_\alpha) + \frac{5}{\bar{\tau}_\beta}G_4(i\bar{\tau}_\beta)\right) - 6G_4(i\bar{\tau}_\beta)H_2'(i\bar{\tau}_\alpha)\right] - \left[G_4(i\bar{\tau}_\alpha) + \frac{5\bar{\tau}_\alpha}{\bar{\tau}_\beta}G_4(i\bar{\tau}_\alpha)\right][\bar{\tau}_\alpha H_2(\bar{\tau}_\beta) - G_2(i\bar{\tau}_\beta)H_2'(i\bar{\tau}_\alpha)] + H_2(\bar{\tau}_\alpha)\left[6G_4(i\bar{\tau}_\beta)\bar{\tau}_\alpha - G_2(i\bar{\tau}_\beta) \times\left[-G_4'(i\bar{\tau}_\alpha) + \frac{5}{\bar{\tau}_\beta}G_4(i\bar{\tau}_\beta)\right]\right]\right\}. \quad [B.5]$$

APPENDIX C: NOTATION

$\tilde{a}_1, \tilde{a}_3$	semiaxes of the solid spheroid
a_1, a_3	dimensionless semiaxes of the solid spheroid
$\tilde{b}_1, \tilde{b}_3$	semiaxes of the spheroidal envelope
b_1, b_3	dimensionless semiaxes of the spheroidal envelope
$\tilde{c}$	semifocal distance of the prolate spheroid
c	dimensionless semifocal distance of the prolate spheroid
$\tilde{\bar{c}}$	semifocal distance of the oblate spheroid
$\bar{c}$	dimensionless semifocal distance of the oblate spheroid
$\tilde{c}_A$	concentration of component A
c_A	dimensionless concentration of component A [$= \tilde{c}_A/\tilde{c}_{A,\infty}$]
$\tilde{c}_{A,\infty}$	concentration of component A far away from the solid spheroid
$\tilde{c}_{A,s}$	concentration of component A upon the solid spheroidal surface
$D, \bar{D}$	determinants defined in Dassios *et al.* (8)
$\tilde{\mathcal{D}}_{AB}$	diffusion coefficient
E	coefficient defined by Eq. [14] for prolate case
$\bar{E}$	transformed E for oblate case
e	eccentricity of the prolate spheroid
$\bar{e}$	eccentricity of the oblate spheroid
$\tilde{k}(\zeta)$	mass transfer coefficient defined by Eq. [35]
$k(\zeta)$	dimensionless $\tilde{k}(\zeta)$ [$=\tilde{k}(\zeta)/\tilde{u}$]
$\tilde{k}_o$	overall mass transfer coefficient defined by Eq. [30]
k_o	dimensionless $\tilde{k}_o$
$\tilde{\mathbf{N}}_A$	molar flux of component A
Pe	Peclet number [$=\tilde{u}\tilde{a}_1/\tilde{\mathcal{D}}_{AB}$]
$\tilde{S}_{os}$	surface area of an oblate spheroid
$\tilde{S}_{ps}$	surface area of a prolate spheroid
$\mathrm{Sh}(\zeta)$	local Sherwood number in the prolate case [$=\tilde{a}_1\tilde{k}(\zeta)/\tilde{\mathcal{D}}_{AB}$]
$\overline{\mathrm{Sh}}(\zeta)$	local Sherwood number in the oblate case [$=\tilde{a}_1\tilde{k}_o/\tilde{\mathcal{D}}_{AB}$]
Sh_o	overall Sherwood number in the prolate case
$\overline{\mathrm{Sh}}_o$	overall Sherwood number in the oblate case
$\tilde{u}$	approach velocity
$\mathbf{v}$	dimensionless fluid velocity
v_η	η-component of $\mathbf{v}$
v_θ	θ-component of $\mathbf{v}$
y	variable defined as $y = \tau - \tau_\alpha$ (prolate case)
$\bar{y}$	variable defined as $\bar{y} = \bar{\tau} - \bar{\tau}_\alpha$ (oblate case)
z	dependent variable defined in Eq. [23]
$\bar{z}$	dependent variable defined in Eq. [40]

Greek Letters

α	value of η on the inner spheroidal surface
β	value of η on the outer spheroidal surface
γ	solid volume fraction
$\tilde{\delta}(\zeta)$	diffusion film thickness defined in Eq. [33]
$\delta(\zeta)$	dimensionless diffusion film thickness
ϵ	porosity
ζ	independent variable defined by Eq. [2]
η	spheroidal coordinate
θ	spheroidal coordinate
$\Lambda_2, \Lambda_3, \Lambda_4$	coefficients defined in Dassios *et al.* (8)
$\tilde{\mu}$	fluid viscosity
μ	dimensionless fluid vicosity
$\tilde{\rho}$	fluid density
ρ	dimensionless fluid density
τ	independent variable defined by Eq. [2]
τ_α	value of τ on the inner spheroidal surface
τ_β	value of τ on the outer spheroidal surface

REFERENCES

1. Happel, J., *AIChE J.* **4,** 197 (1958).
2. Kuwabara, S., *J. Phys. Soc. Jpn.* **14,** 527 (1959).
3. Tien, C., "Granular Filtration of Aerosols and Hydrosols," p. 65. Butterworths, Boston, 1989.
4. Neale, G. H., and Nader, W. K., *AIChE J.* **20,** 530 (1974).
5. Brinkman, H. C., *Appl. Sci. Res. Sect. A* **1,** 27 (1947).
6. Neale, G. H., Epstein, N., and Nader, W. K., *Chem. Eng. Sci.* **28,** 1865 (1973).
7. Epstein, N., and Masliyah, J. H., *Chem. Eng. J.* **3,** 169 (1972).
8. Dassios, G., Hadjinicolaou, M., and Payatakes, A. C., *Quart. Appl. Math.*, in press.
9. Pfeffer, R., and Happel, J., *AIChE J.* **10,** 605 (1964).
10. Pfeffer, R., *Ind. Eng. Chem. Fundam.* **3,** 380 (1964).
11. Levich, V. G., "Physicochemical Hydrodynamics," p. 80. Prentice-Hall, Englewood Cliffs, NJ, 1962.
12. Friedlander, S. K., *AIChE J.* **7,** 347 (1961).
13. Lochiel, A. C., and Calderbank, P. H., *Chem. Eng. Sci.* **19,** 471 (1964).
14. Acrivos, A., and Goddard, J. D., *J. Fluid Mech.* **23,** 273 (1965); **24,** 339 (1966).
15. Tardos, G. I., Gutfinger, C., and Abuaf, N., *AIChE J.* **22,** 1147 (1976).
16. Happel, J., and Brenner, H., "Low Reynolds Hydrodynamics," p. 145. Prentice-Hall, Englewood Cliffs, NJ, 1965.